Evidence for Topologically Protected Surface States and a Superconducting Phase in $[Tl_4](Tl_{1-x}Sn_x)Te_3$ Using Photoemission, Specific Heat, and Magnetization Measurements, and Density Functional Theory

K. E. Arpino,[1,2] D. C. Wallace,[1,2] Y. F. Nie,[3,4] T. Birol,[5] P. D. C. King,[3,6] S. Chatterjee,[3] M. Uchida,[3] S. M. Koohpayeh,[2] J.-J. Wen,[2] K. Page,[7] C. J. Fennie,[5] K. M. Shen,[3,6] and T. M. McQueen[1,2,*]

[1]*Department of Chemistry, The Johns Hopkins University, Baltimore, Maryland 21218, USA*

[2]*Institute for Quantum Matter, Department of Physics and Astronomy, The Johns Hopkins University, Baltimore, Maryland 21218, USA*

[3]*Department of Physics, Laboratory of Atomic and Solid State Physics, Cornell University, Ithaca, New York 14853, USA*

[4]*Department of Materials Science and Engineering, Cornell University, Ithaca, New York 14853, USA*

[5]*School of Applied and Engineering Physics, Cornell University, Ithaca, New York 14853, USA*

[6]*Kavli Institute at Cornell for Nanoscale Science, Cornell University, Ithaca, New York 14853, USA*

[7]*Lujan Neutron Scattering Center, Los Alamos National Laboratory, Los Alamos, New Mexico 87545, USA*

(Received 19 August 2013; published 8 January 2014)

We report the discovery of surface states in the perovskite superconductor $[Tl_4]TlTe_3$ (Tl_5Te_3) and its nonsuperconducting tin-doped derivative $[Tl_4](Tl_{0.4}Sn_{0.6})Te_3$ as observed by angle-resolved photoemission spectroscopy. Density functional theory calculations predict that the surface states are protected by a Z_2 topology of the bulk band structure. Specific heat and magnetization measurements show that Tl_5Te_3 has a superconducting volume fraction in excess of 95%. Thus Tl_5Te_3 is an ideal material in which to study the interplay of bulk band topology and superconductivity.

DOI: 10.1103/PhysRevLett.112.017002 PACS numbers: 74.25.-q, 73.20.-r, 73.43.-f

Charge carriers in Dirac-like bands have a linear energy-momentum relationship described by the Dirac equation; they offer the unique opportunity to investigate the intersection of special relativity and quantum mechanics. However, materials exhibiting Dirac-like states are relatively rare, the most notable examples being graphene [1], Z_2 topological insulators [2], and topological crystalline insulators [3]. Materials which combine nontrivial band topologies with superconductivity have the ability to test the predictions of new states of matter and open the field for new technologies such as quantum computing [4–7], but producing such materials has been a challenge [8–10].

In this Letter, we report the discovery of Dirac-like surface states in $[Tl_4](Tl_{1-x}Sn_x)Te_3$, as observed by angle-resolved photoemission spectroscopy (ARPES). Density functional theory (DFT) predicts these surface states to be Z_2 topologically protected due to a spin-orbit-driven band parity inversion at the Z time reversal invariant momentum point of the first Brillouin zone. Specific heat and magnetization measurements show that Tl_5Te_3 exhibits fully gapped, bulk superconductivity below $T_c = 2.40(1)$ K with a 96% volume fraction.

The $[Tl_4]MTe_3$ (M = Tl, Sn, Pb, Bi, Sb, La, Nd, and Mo [11–14]) compounds have a tetragonal perovskite structure (ABO_3), shown in Fig. 1(a) [15]. The cavities of a three-dimensional network of corner-sharing MTe_6 octahedra are occupied by interconnected Tl_4 tetrahedra. There are several ways in which the $[Tl_4]MTe_3$ structure can produce topologically protected surface states. First, the mirror planes which protect surface states in rock salt topological crystalline insulators such as SnTe are also present in the basic perovskite structure of this family; the appropriate band inversions at points protected by mirror symmetry similarly may yield a topological crystalline insulator state in body-centered tetragonal symmetry. Second, the body-centered tetragonal crystal class of $[Tl_4]MTe_3$ structure has four sets of time-reversal invariant points: one Γ, four N, two X, and one Z. If spin-orbit coupling produces an odd number of band parity inversions, e.g., a single inversion at either the Γ or Z point, but not both, strong Z_2 topologically protected surface states would result [18].

To check these possibilities, first principles (DFT) calculations were performed with full-potential linear augmented wave formalism as implemented in WIEN2K [19]. Exchange-correlation energies are calculated with Perdew-Burke-Erzenhof functional [20]. An $8 \times 8 \times 8$ unshifted k-point grid is used in the Brillouin zone of the primitive body-centered tetragonal cell. Results reported were double checked by repeating calculations in projector augmented wave formalism, as implemented in VASP, and no disagreements were found [21]. The $I4/mcm$ cell used for the calculations was determined by Rietveld refinements to neutron powder diffraction data collected on Tl_5Te_3 at $T = 295$, 100, and 15 K on the NPDF instrument at the Los Alamos Neutron Science Center, which show no evidence of a structural transition down to $T = 15$ K. These data are consistent with the structural data obtained from synchrotron x-ray diffraction at higher temperatures. Our DFT calculations for Tl_5Te_3, shown in Figs. 1(c) and 1(d), show spin-orbit coupling

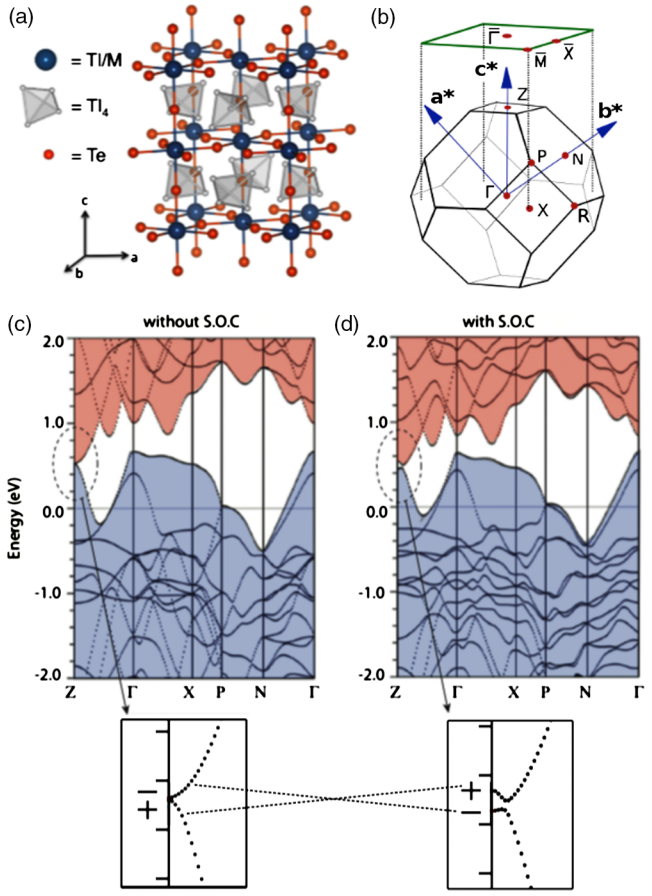

FIG. 1 (color online). (a) Tl_5Te_3 consists of Tl_4 tetrahedra occupying the A site of a conventional perovskite ABO_3, the corner-sharing lattice of $(Tl/M)Te_6$ octahedra alternatingly rotated by 20.1° about the c axis ($a^0a^0c^-$ in Glazer notation) [15–17]. (b) The Brillouin zone of the body-centered tetragonal unit cell, and its two-dimensional projection, is shown. The band structure of Tl_5Te_3, calculated from first principles DFT both without (c) and with (d) spin-orbit interactions. Shading denotes bands arising from valence (blue) and conduction (pale red) band states. The spin-orbit interaction produces a single band parity inversion at the Z point, indicating that Tl_5Te_3 would be a topological semimetal if doped to the gap. Band parities are indicated by + and − signs.

induces a single band inversion between valence and conduction band states at the Z point approximately 0.5 eV above the calculated Fermi level. This inversion is between opposite-parity states, the conduction band involving states from the $[Tl_4]$ units on the A site and the valence band involving mainly states from apical Te atoms and B-site Tl ions in the corner-sharing perovskite network. If electron doped up to the gap at Z, this system would be a topological semimetal due to high-lying valence band states at the Γ point. The resulting situation is thus similar to that found in pure antimony, which is a semimetal with topologically protected surface states that becomes a topological insulator when doped with Bi [22]. To confirm the nontrivial bulk band topology, we have calculated the Z_2 invariant to be −1 by taking the product of the parity of all the bands at the Γ and Z points that connect to the occupied valence bands, including two bands above the Fermi level at the Γ point. Therefore, DFT predicts Tl_5Te_3 to have surface states protected by a nontrivial Z_2 topology.

To confirm this prediction experimentally, we have synthesized crystals of Tl_5Te_3 and related electron-doped compounds, and have studied their electronic structure using ARPES. Polycrystalline Tl_5Te_3 samples were prepared by heating elemental Tl (Strem Chemicals, 99.9%) and Te (Alfa Aesar, 99.999 + %) in a vacuum-sealed silica ampoule to 550°C, holding for 24 h, followed by slow cooling (5°C/h). Elemental thallium was stored and handled in an inert atmosphere to prevent oxidization. Single crystals were prepared using a modified Bridgman method in an optical floating-zone furnace (Crystal Systems) using 2.5% excess Te as a flux. $[Tl_4](Tl_{1-x}Sn_x)Te_3$ samples were prepared by heating elemental Tl, Te, and Sn (NOAH Technologies, 99.9%) in a vacuum-sealed silica ampoule to 540°C, holding for 24 h, followed by slow cooling (2°C/h). Single crystals of $[Tl_4](Tl_{0.4}Sn_{0.6})Te_3$ suitable for ARPES measurements were obtained from the ingot after slow cooling. Compositions of the single crystals were assumed to be homogenous with the bulk ingot, the composition of which was determined by comparison to Rietveld refinement of high-resolution synchrotron x-ray diffraction data.

ARPES measurements were performed at the Synchrotron Radiation Center in Wisconsin at the U3 beam line with a VG Scienta R4000 electron analyzer at a base temperature of 30 K and a pressure of 8×10^{-11} torr as well as a lab-based ARPES system with a VG Scienta R4000 analyzer and VUV5000 helium plasma discharge lamp ($h\nu = 21.2$ and 40.8 eV) and monochromator at a temperature of 20 K and a base pressure of 6×10^{-11} torr. Samples were cleaved *in situ* along the c axis in ultrahigh vacuum in order to expose atomically clean surfaces.

In Fig. 2, we show ARPES data for Tl_5Te_3 and $[Tl_4](Tl_{0.4}Sn_{0.6})Te_3$, measured at $T = 20$ and 30 K using a helium discharge lamp and monochromatic synchrotron radiation. The most prominent feature in each case is an intense, linearly dispersing (Dirac-like) band centered at a momentum of ($k_x = 0$, $k_y = 0$) of the two-dimensional surface Brillouin zone (2DBZ). The projection from bulk to surface Brillouin zone is illustrated in Fig. 1(b). We observe this feature at the center of numerous 2DBZs, and only a single such feature in each zone. We identify this feature as a surface state based on several distinct pieces of evidence. First, the values of its extracted Fermi velocity and Fermi wave vector are insensitive to incident photon energy in both compounds, indicating that these states are nondispersive in k_z, characteristic of a surface state [Figs. 2(d) and 2(g)]. In contrast, we additionally observe broad diffuse bands showing substantial changes

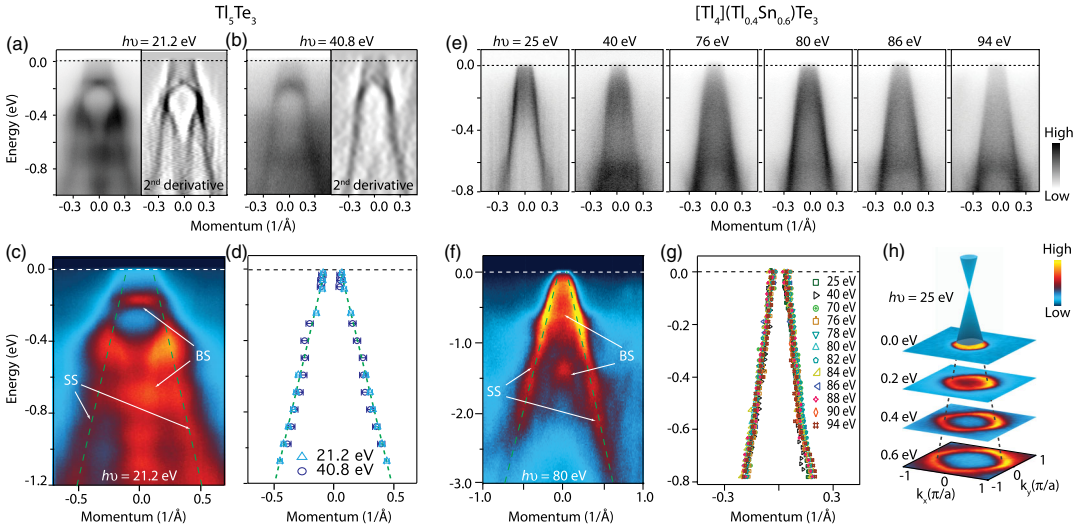

FIG. 2 (color online). Plots of ARPES intensity as a function of binding energy and crystal momentum in the (0,0) – (π,π) direction of Tl_5Te_3 measured using photon energies of (a), (c) 21.2 eV and (b) 40.8 eV show a linearly dispersing surface state (SS, highlighted with green dashed lines) coexisting with additional bulk states (BS). Visualization of the surface state is improved by taking the second derivative with respect to momentum [right panels in (a) and (b)]. (d) Extracted dispersion of the surface state from fits to momentum distribution curves for Tl_5Te_3. These show no dependence on the incident photon energy (i.e., no k_z dependence). Similar features are observed in $[Tl_4](Tl_{0.4}Sn_{0.6})Te_3$: (e) photon energy-dependent measurements reveal a single linear surface state which does not change with varying photon energy [see (g)], while bulk states disperse with k_z to give filled intensity inside the Dirac cone. (f) The surface state evolves into a surface resonance at higher binding energies, where additional bulk electronic states are visible. (h) Isoenergy plots of intensity versus momentum in the k_x-k_y plane illustrate the presence of a single Dirac cone centered at the origin of the 2DBZ in $[Tl_4](Tl_{0.4}Sn_{0.6})Te_3$. The Dirac cone exhibits fourfold warping away from the Dirac point, consistent with the tetragonal crystal symmetry of these materials.

with photon energy, as expected for bulk valence bands which disperse strongly along k_z. These observed bulk states are consistent with both the three-dimensional structure of these compounds as well as our first-principles calculations. Furthermore, the Dirac-like feature is present and always centered at (0,0) of the 2DBZ, rather than the center of the three-dimensional bulk Brillouin zone as would be expected for a bulk-derived state.

The surface state shows no detectable Rashba-type spin splitting despite the strong spin-orbit coupling of these materials, a fact which strongly suggests that the surface state is spin polarized. The existence of a single such non-spin-degenerate Dirac cone centered at the (0,0) time-reversal invariant point of the surface Brillouin zone is a hallmark of a surface state protected by a Z_2 topology. As such, our measurements provide direct experimental evidence for the existence of topologically protected surface states in both Tl_5Te_3 and $[Tl_4](Tl_{0.4}Sn_{0.6})Te_3$. First principles DFT calculations support this conclusion, establishing $[Tl_4](Tl_{1-x}Sn_x)Te_3$ as an entirely new materials system hosting topologically nontrivial phases.

The topological surface states display a number of attractive features. First, as in the bismuth chalcogenide topological insulators, there is only a single topological state per surface Brillouin zone in Tl_5Te_3 and $[Tl_4](Tl_{0.4}Sn_{0.6})Te_3$ [23]. For both compounds, only the bottom section of the Dirac cone is visible, and the extrapolated Dirac point sits 0.21(1) and 0.20(2) eV above the Fermi level for Tl_5Te_3 and $[Tl_4](Tl_{0.4}Sn_{0.6})Te_3$, respectively. The Dirac cones exhibit a fourfold warping away from the Dirac point consistent with the materials' tetragonal symmetry [Fig. 2(h)], akin to the sixfold warping in known trigonal topological insulators [24]. Second, alloying Sn for Tl proves to be an effective method to modify the surface state dispersion: the extracted Fermi velocity of 3.0(2) eV Å for Tl_5Te_3 increases to 4.6(2) eV Å in $[Tl_4](Tl_{0.4}Sn_{0.6})Te_3$, and the wave vector correspondingly decreases from 0.07(1) to 0.04(1) $Å^{-1}$. Finally, the surfaces of these compounds appear to be more robust against the effects of adsorbates than in bismuth chalcogenides [25], with no significant time- or pressure-dependent changes of this doping level observed during ARPES measurements, which may prove to be an attractive feature for utilizing these surface states in future applications.

In addition to harboring Dirac-like surface states, Tl_5Te_3 is a bulk superconductor [26,27]. Physical property measurements were performed on a Quantum Design, Inc. Physical Property Measurement System. Low-temperature heat capacity data from $T = 0.15$ to 4 K were collected with the aid of a dilution refrigerator. Specific heat data collected on a polycrystalline flake under zero magnetic field reveal a clear λ anomaly, shown in Fig. 3(a). An equal-entropy construction indicates bulk superconductivity with $T_c = 2.40(1)$ K. The

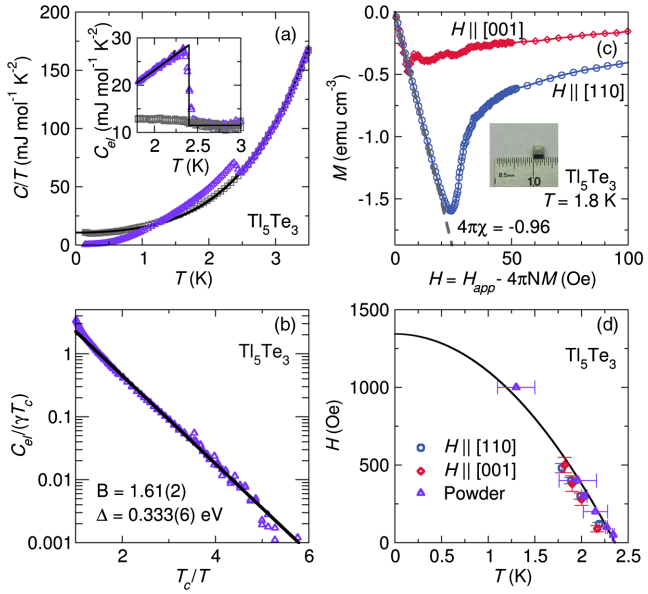

FIG. 3 (color online). (a) Specific heat data collected under zero magnetic field (purple triangles) show a clear λ anomaly at $T_c = 2.40(1)$ K, with a $H = 5$ kOe field sufficient to quench superconductivity. (b) Low-temperature electronic specific heat shows fully gapped behavior. (c) Isothermal magnetization data collected on an oriented single crystal at $T = 1.8$ K with the field applied parallel to the [001] direction (red diamonds) and [110] direction (blue circles) reveal anisotropy of H_c^*. A demagnetization factor of $N = 1/3$ has been applied to account for the approximately cubic shape of the 100 mg single crystal sample (inset). (d) The field-temperature phase diagram shows H_{c2} as determined by specific heat (purple triangles) and orientation-dependent isothermal dc magnetization (blue circles and red diamonds), along with a two-fluid model fit to the data.

ratio $\Delta C_{el}/(\gamma T_c) = 1.63$ is close to the weak coupling Bardeen-Cooper-Schrieffer (BCS) value of 1.43 [28]. Low-temperature specific heat measurements collected under $H = 0$ Oe and 5 kOe show the latter field is sufficient to quench superconductivity. The data collected under a $H = 5$ kOe field below $T = 1.5$ K, temperatures at which any complex phonon structure should be negligible, were fit to $C_{el} = \gamma T + \beta_3 T^3$, where $\gamma = 9.34(4)$ mJ mol f.u.$^{-1}$ K^{-2} and $\beta_3 = 6.82(5)$ mJ mol f.u.$^{-1}$ K^{-4} [29], which corresponds to a Debye temperature of $\Theta_D = 132(1)$ K [29]. Subtracting this low-temperature lattice specific heat fit gives the electronic specific heat, which is well described by the BCS model of the electronic specific heat of a single-gap s-wave superconductor $C_{el}/(\gamma T_c) = A \exp[(-BT_c)/T]$ with $A = 11.4(1.1)$ and $B = 1.61(2)$, which holds for $T_c/T \gtrsim 2$ [Fig. 3(b)] [28,29]. According to BCS theory, $B = \Delta k_B T_c$, and thus a value of $B = 1.61(2)$ predicts a superconducting gap of $\Delta = 0.333(6)$ meV. This value, based on the electronic specific heat data, agrees with the superconducting gap of $\Delta = 0.365(2)$ meV predicted using the critical temperature of $T_c = 2.40(1)$ K in the BCS relation $2\Delta/(k_B T_c) = 3.53$. These specific heat measurements indicate a Tl_5Te_3 is a fully gapped bulk superconductor, a prerequisite for a topological superconductor [6].

Isothermal dc magnetization measurements reveal a superconducting volume fraction in excess of 95% at $T = 1.8$ K under small applied magnetic field applied along either the [001] and [110] crystal directions [Fig. 3(c)]. The directional upper critical fields are the same within error [Fig. 3(d)], while the lower critical fields are found to differ by a factor of greater than three [Fig. 3(c)]. This difference in anisotropy between upper and lower critical fields is unexpected based on the Ginzburg-Landau equations, and is not due to a demagnetization effect. While we cannot rule out other explanations, in light of the ARPES results it seems likely that this discrepancy arises from the presence of Dirac-like surface states that change the effective screening of the applied magnetic field.

Our results show that the bulk superconductor Tl_5Te_3 has Dirac-like surface states. Further, our ARPES results show that these surface states survive in the tin-doped derivative, $[Tl_4](Tl_{0.4}Sn_{0.6})Te_3$. Because Sn favors a 2+ oxidation state, it is isovalent with the Tl^{2+} it is replacing and thus the electronic structure is not greatly affected. Upon doping with tin, the primary experimental effects observed are an increase in the dispersion of the surface state, with only a small change in the position of the Fermi level relative to the extrapolated position of the Dirac point. DFT calculations on $[Tl_4]SnTe_3$ (not shown) explain these observations. In contrast to Tl_5Te_3, in $[Tl_4]SnTe_3$ a ~0.7 eV band gap is predicted at the Z point; i.e., the separation between the valence and conduction bands increases with increasing x in $[Tl_4](Tl_{1-x}Sn_x)Te_3$, and prevents spin orbit coupling from inducing a band parity inversion. Consequently, for some value of x in the $[Tl_4](Tl_{1-x}Sn_x)Te_3$ series, there is a topological phase transition, similar to what is found for the $Bi_{1-x}Sb_x$ solid solution [22]. As long as x is less than the threshold value, the spin-orbit driven band inversion is maintained, but there the dispersion of the surface state increases with increasing x, as experimentally observed. The position of the Fermi level relative to the Dirac point then changes little because, even though electrons are being added to the system, the number of states per unit energy is decreasing due to the increased dispersion.

The presence of Dirac-like surface states implies a nontrivial band topology, and Tl_5Te_3 is an intrinsic, stoichiometric, bulk superconductor that is straightforward to synthesize and computationally model. Further, the discovery of topological surface states in the $[Tl_4]MTe_3$ family has broader implications in the field of topological insulator research: this family has an entirely different crystal structure than the known Z_2 topological insulators, which all have trigonal symmetry in the active units. The wide range of cations reported to substitute for the M site (and anions

for tellurium) present a versatile range of experimentally accessible doping levels and resultant properties to examine. For example, preliminary calculations (not shown) indicate that the topological nature of $[Tl_4]MTe_3$ is very sensitive to structural parameters, suggesting that temperature-, pressure-, and/or strain-induced topological transitions may also exist in this material family. In short, our discovery of topological surface states in the $[Tl_4]MTe_3$ family is the first observation of Dirac-like surface states in the largest known material structure type, perovskites, and Tl_5Te_3 has both Z_2 topological surface states and high volume fraction bulk superconductivity.

T. M. M. acknowledges support of startup funds from the Johns Hopkins University as well as the David and Lucile Packard Foundation. K. M. S. acknowledges the NSF Materials Research Science and Engineering Centers (MRSEC) program Grant No. DMR-1120296, AFOSR Grants No. FA9550-11-1-0033 and No. FA9550-12-1-0335, and the NSF CAREER Grant No. DMR-0847385. T. B. was supported as part of the Energy Materials Center at Cornell (EMC^2), an Energy Frontier Research Center funded by the U.S. Department of Energy, Office of Science, Office of Basic Energy Sciences under Award No. DE-SC0001086. C. J. F. was supported by the Cornell Center for Materials Research with funding from the NSF MRSEC program (DMR-1120296). Crystal growth supported by DOE, Office of Science, Basic Energy Sciences, Division of Materials Sciences and Engineering (The Institute for Quantum Matter, Award No. DE-FG02-08ER46544). This work has benefited from the use of the NPDF beam line at the Lujan Center at Los Alamos Neutron Science Center, funded by the U.S. DOE Office of Basic Energy Sciences. Los Alamos National Laboratory is operated by Los Alamos National Security LLC under DOE Contract No. DE-AC52-06NA25396. The dilution refrigerator used in this study was funded through the National Science Foundation Major Research Instrumentation Program, Grant No. DMR-0821005. K. E. A., D. C. W., and Y. F. N. contributed equally to this work.

*mcqueen@jhu.edu

[1] A. K. Geim and K. S. Novoselov, Nat. Mater. **6**, 183 (2007).
[2] L. Fu, C. L. Kane, and E. J. Mele, Phys. Rev. Lett. **98**, 106803 (2007).
[3] L. Fu, Phys. Rev. Lett. **106**, 106802 (2011).
[4] A. C. Potter and P. A. Lee, Phys. Rev. B **85**, 094516 (2012).
[5] J. Linder, Y. Tanaka, T. Yokoyama, A. Sudbo, and N. Nagaosa, Phys. Rev. Lett. **104**, 067001 (2010).
[6] J. D. Sau, R. M. Lutchyn, S. Tewari, and S. Das Sarma, Phys. Rev. B **82**, 094522 (2010).
[7] S. Tewari, T. D. Stanescu, J. D. Sau, and S. Das Sarma, New J. Phys. **13**, 065004 (2011).
[8] G. Koren, T. Kirzhner, E. Lahoud, K. B. Chashka, and A. Kanigel, Phys. Rev. B **84**, 224521 (2011).
[9] Y. S. Hor, A. J. Williams, J. G. Checkelsky, P. Roushan, J. Seo, Q. Xu, H. W. Zandbergen, A. Yazdani, N. P. Ong, and R. J. Cava, Phys. Rev. Lett. **104**, 057001 (2010).
[10] S. Sasaki, Z. Ren, A. A. Taskin, K. Segawa, L. Fu, and Y. Ando, Phys. Rev. Lett. **109**, 217004 (2012).
[11] Y. V. Voroshilov, M. I. Gurzan, Z. Z. Kish, and L. V. Lada, Neorg. Mater. **24**, 1479 (1988).
[12] S. Bangarigadu-Sanasy, C. R. Sankar, A. Assoud, and H. Kleinke, Dalton Trans. **40**, 862 (2011).
[13] S. Z. Imamalieva, F. M. Sadygov, and M. B. Babanly, Inorg. Mater. (USSR) **44**, 935 (2008).
[14] S. Bradtmöller, and P. Böttcher, Z. Kristallogr. **209**, 75 (1994).
[15] P. Böttcher, T. Doert, C. Druska, and S. Bradtmöller, J. Alloys Compd. **246**, 209 (1997).
[16] A. M. Glazer, Acta Crystallogr. Sect. B **28**, 3384 (1972).
[17] K. Momma and F. Izumi, J. Appl. Crystallogr. **44**, 1272 (2011).
[18] L. Fu and C. L. Kane, Phys. Rev. B **76**, 045302 (2007).
[19] P. Blaha, K. Schwarz, G. K. H. Madsen, D. Kvasnicka, and J. Luitz, *WIEN2K: An Augmented Plane Wave + Local Orbitals Program for Calculating Crystal Properties* (Vienna University of Technology, Vienna, Austria, 2001).
[20] J. P. Perdew, K. Burke, and M. Ernzerhof, Phys. Rev. Lett. **77**, 3865 (1996).
[21] G. Kresse and J. Furthmüller, Phys. Rev. B **54**, 11169 (1996).
[22] S Hsieh, D. Qian, L. Wray, Y. Xia, Y. S. Hor, R. J. Cava, and M. Z. Hasan, Nature (London) **452**, 970 (2008).
[23] H. Zhang, C.-X. Liu, X.-L. Qi, X. Dai, Z. Fang, and S.-C. Zhang, Nat. Phys. **5**, 438 (2009).
[24] Y. L. Chen *et al.*, Science **325**, 178 (2009).
[25] M. Bianchi, D. Guan, S. Bao, J. Mi, B. B. Iversen, P. D. C. King, and P. Hofmann, Nat. Commun. **1**, 128 (2010).
[26] A. Juodakis and C. R. Kannewurf, J. Appl. Phys. **39**, 3003 (1968).
[27] W. H. Haemmerle, W. A. Reed, A. Juodakis, and C. R. Kannewurf, J. Appl. Phys. **44**, 1356 (1973).
[28] J. C. Bardeen, L. N. Cooper, and J. R. Schrieffer, Phys. Rev. **108**, 1175 (1957).
[29] A Tari, *The Specific Heat of Matter at Low Temperatures.* (Imperial College Press, London, 2003).